View metadata, citation and similar papers at core.ac.uk

brought to you by CORE

provided by Scholarly Materials And Research @ Georgia Tech

# Zinc Oxide coated Carbon Nanotubes as Piezoelectric Nanogenerators

An Undergraduate Thesis
Presented to
The Academic Faculty

by

Celeste Mason

In Partial Fulfillment
of the Requirements for the
Undergraduate Research Option

Advisor: Dr. David W. Stollberg

School of Materials Science and Engineering

December 11th, 2009

## Table of Contents:

## Research Description & Literature Review

**Motivation:**

Numerous new electronically based products and ideas are currently in development for recreational, corporate, military, and medical use. As research progresses, so too does the increase in power and reduction in size of electronic devices. One of the greatest challenges in the development of micromechanical and nanoscale systems, as well as biomedical components and sensors is the lack of an efficient power source of similar scale.

Many of these devices are designed to be portable. This requires a constant renewal of their power sources—batteries that will either be inevitably depleted, or must be recharged from a fixed source. Due to these limitations, the dependence of these devices on batteries is a major drawback. For example, biomedical implants that must have their batteries exchanged, or electronics used by military personnel that require the additional transport of batteries and charging devices—both exposing the user to increased risk.

A viable solution would be a scalable power source that draws its energy from the surrounding environment and does not need to be replaced or recharged. There have been numerous devices proposed that would transform mechanical energy to electrical energy through use of transducers. These are often composed of piezoelectric materials with a variety of structures—primarily ceramics such as lead zirconate titanate (PZT), zinc oxide (ZnO) and even some polymers [1-17].

Such devices may also be created by coating carbon nanotubes (CNTs) with a piezoelectric substance such as ZnO. In this configuration, the electrical and mechanical versatility of carbon nanotubes would permit them to act as a strong, flexible, conductive substrate that would not only support the ZnO coating, but would also allow fast and efficient collection of charge produced by elastic deformation of ZnO (Figure 1) [18].

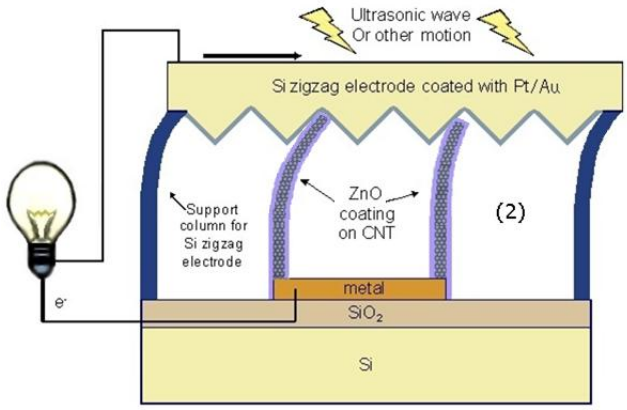


Figure 1. ZnO-coated CNT based piezoelectric nanogenerator, adapted from [18]

This configuration is similar to one developed by Zhong Lin Wang's research group at the Georgia Institute of Technology, who rely on piezoelectric ZnO nanowires alone in an array of nanogenerator configurations [19-34]. When a piezoelectric nanogenerator is placed in an environment where it encounters sound or other vibrations the piezoelectric structures may be deformed by the conductive electrode, imparting stress, which induces a charge gradient (Figure 2) [20].

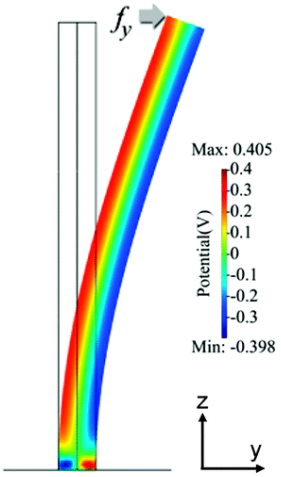


Figure 2. Potential induced by applied force to ZnO nanostructure [20]

When the side of a charged ZnO nanowire or ZnO-coated nanotube contacts the gold surface, it forms a Schottky barrier. A charge transfer occurs which may

proceed in one direction only—from the ZnO to the gold coated electrode—producing an electrical current (Figure 3).

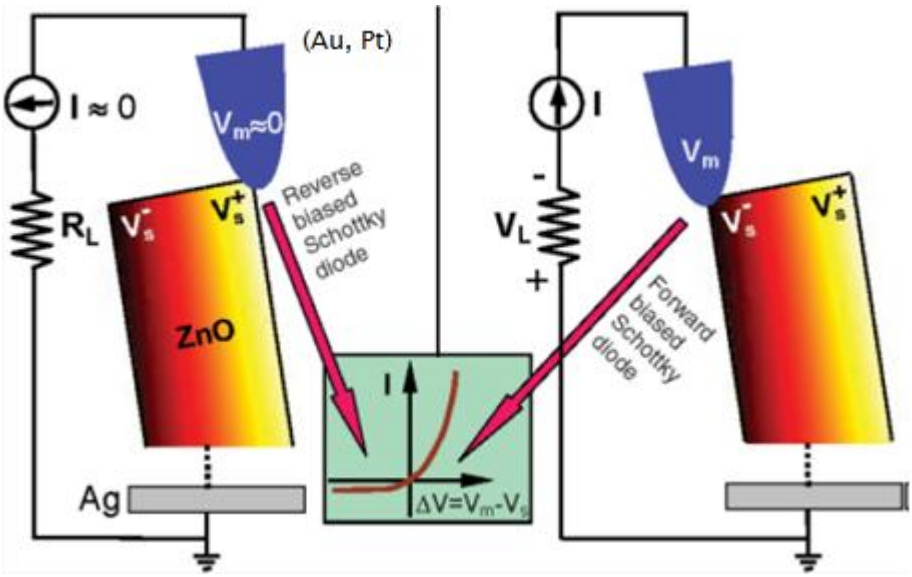


Figure 3. Charge is dissipated when in the forward Schottky diode region of I-V curve, adapted from [34]

**Materials:**

A carbon nanotube can essentially be thought of as a sheet of graphene rolled to form a cylinder with the edges joined along the length and capped with hemispherical fullerenes [35]. The angle at which a CNT is rolled determines whether it displays conductive or semiconductive properties (Figure 4) [18].

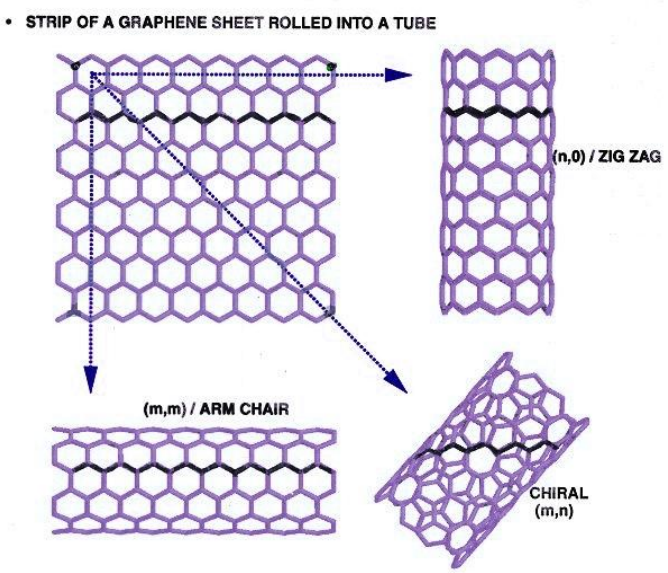


Figure 4. CNT structure variations, adapted from [18]

Electrical properties also vary with the diameter of the CNT or whether it is encased in successive concentric layers. These are referred to as multi-walled carbon nanotubes (MWCNTs) as opposed to single walled carbon nanotubes (SWCNTs). These variations in CNT structure and properties can be controlled during growth by the application of an electric field or the adjustment of the precursor gas recipe during the chemical vapor deposition (CVD) process [36].

The difference in scale of CNTs in relation to ZnO nanowires must be addressed when designing a device that relies on the mechanical behavior of a material. The CNTs consistently grown for this project are approximately 60μm in length, with a range of diameters of approximately 3-20nm depending on number of walls. The ZnO nanowires used in Dr. Z.L. Wang's nanogenerators are approximately 1μm in length and 40nm in diameter [19].

Until recently, CNTs have only been reproducibly grown using the standard CVD process as long filaments in dense mats or "carpets". The CNTs in this study were grown by standard CVD; however, CNTs may be grown with spacing by plasma CVD. In contrast, ZnO nanowires have smaller aspect ratios and can be grown with greater spacing between individual wires. Adequate space between the individual wires is required in order for the opposite

(Schottky) electrode to isolate and deform the wire (producing the charge) as well as to position it in contact with a conductive metal such as gold that forms a Schottky barrier.

The potential for a material to exhibit piezoelectric behavior is dependent on the relative deviation of its crystal lattice from symmetry [37]. When a mechanical force deforms the material and shifts its center of charge, the charge is separated towards opposing sides of the material. Most materials will not exhibit identical piezoelectric behavior along differing crystallographic directions. The degree of piezoelectricity is dependent on the material's composition and crystal orientation, and defined is by the piezoelectric constitutive equations:

$$\mathbf{S} = \mathbf{s}_{\mathbf{E}} \cdot \mathbf{T} + \mathbf{d}^{t} \cdot \mathbf{E}$$

$$\mathbf{D} = \mathbf{d} \cdot \mathbf{T} + \boldsymbol{\varepsilon}_{\mathbf{T}} \cdot \mathbf{E}$$

where S is strain, T is stress, D is charge density displacement, E is the electric field, d is the matrix containing the piezoelectric constants,  is a matrix of compliance coefficients and E is the electrical permittivity.

The piezoelectric behavior of ZnO, which has a hexagonal wurtzite crystal structure, is dependent on its lattice orientation relative to the substrate surface. ZnO produces the greatest amount of charge along its <002> axis [37]. As a result, any attempt at creation of a film or features for use in piezoelectric applications requires that the deposition or growth process be optimized to maximize the amount of <002> axis ZnO along the path forming the electrical circuit. ZnO nanowires are routinely grown with their <002> axis aligned along the length of the wires, which are perpendicular to the substrate on which they are grown. They exhibit single crystal growth, which further improves their ability to produce charge. The ZnO-coated CNT configuration, the CNT surfaces are (on average) perpendicular to the substrate used for the ZnO nanowire approach. This may result in a different relative orientation of the ZnO crystal

structure to the substrate surface. Further adjustment of the methods of deformation and the collection of charge produced may be required.

It is not yet known whether crystalline growth behavior similar to that of the ZnO nanowires will be present in films of ZnO deposited on CNTs by each of the techniques being considered. Preliminary analysis by transmission electron microscopy (TEM), however, shows a trend toward preferred orientation of polycrystalline ZnO deposited by radio frequency (RF) sputtering (Figure 5) [38].

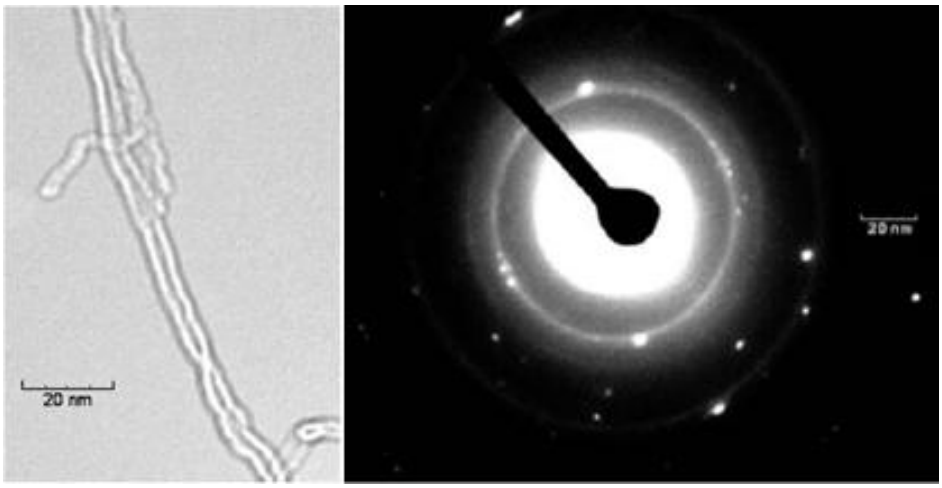


Figure 5. TEM images of ZnO-coated CNTs grown on carbon fiber (left) and an electron diffraction pattern displaying some preferred orientation (right) [38]

**Processing:**

Many methods of deposition of ZnO onto CNTs were considered: RF sputtering, flame-assisted CVD, thermal evaporation, sol-gel coating, atomic layer deposition (ALD), ion-assisted deposition (IAD), and the standard CVD process [39]. These methods were researched and compared to determine the process that would produce the best quality film. Few of the proposed methods have been shown to produce epitaxial films on CNTs. RF sputtering, IAD, evaporation, and other physical vapor deposition methods produce rough, polycrystalline coatings. These coatings are predominantly of c-axis orientation. Sol-gel synthesis of ZnO can result in a porous film, nanocrystallites, and other structures, with varied crystal orientations depending on precursor and post-deposition annealing [40-42]. Results were predominantly obtained from

experimental processes normally performed on flat substrates, such as glass via spin coating. Deposition of ZnO on CNTs by sol-gel would be likely to produce undesired morphologies of the CNT carpet due to the effect of spin coating combined with the wicking tendency of CNTs. Evaporation of pure zinc metal, or solid ZnO particles in a tube furnace is a possible means of deposition of ZnO on CNTs. This results in nanowire or complex nanoneedle structures [43-44]. CVD or ALD methods may be most likely to provide complete coating coverage with the highest degree of desired crystal orientation. The processes compared in this study are IAD and RF sputtering due to the possibility that the ionized ZnO may be propelled further into the CNT carpet, producing a more conformal coating.

## Experimental Procedure

### Design:

The design of the piezoelectric generator is based upon two primary approaches: use of a rigid and a flexible substrate. For the piezoelectric electrode using a rigid substrate, vertically aligned CNTs are grown on an iron-coated silicon wafer by pyrolysis of hydrocarbon gas in a CVD chamber. The CNTs are then coated with ZnO via a variety of physical or chemical deposition processes. The CNTs may alternately be patterned into arrays by photolithographic processing to improve spacing—increasing potential for deformation when stressed and, consequently, power generation.

A second silicon wafer, to be used as a conductive electrode, may either be etched into a periodic zigzag pattern of triangular peaks and valleys [45] in directions perpendicular to the nanotubes' substrate (Figure 6a) or coated with an iron catalyst, in order to grow CNTs for use as a substrate (Figure 6b). The CNTs may also be photolithographically patterned into arrays. Using any of these methods, a top electrode may be formed that is then coated with gold or platinum. When the top and bottom electrodes are combined to form a circuit, the top wafer will act as the trigger and an electron sink for the ZnO as its

piezoelectric behavior is induced by ambient vibrations/energy present in the environment. The variation of morphology of the substrates will provide a means of comparing the ability of the electrode to isolate and deform the individual ZnO-coated CNTs, while forming an efficient Schottky barrier contact.

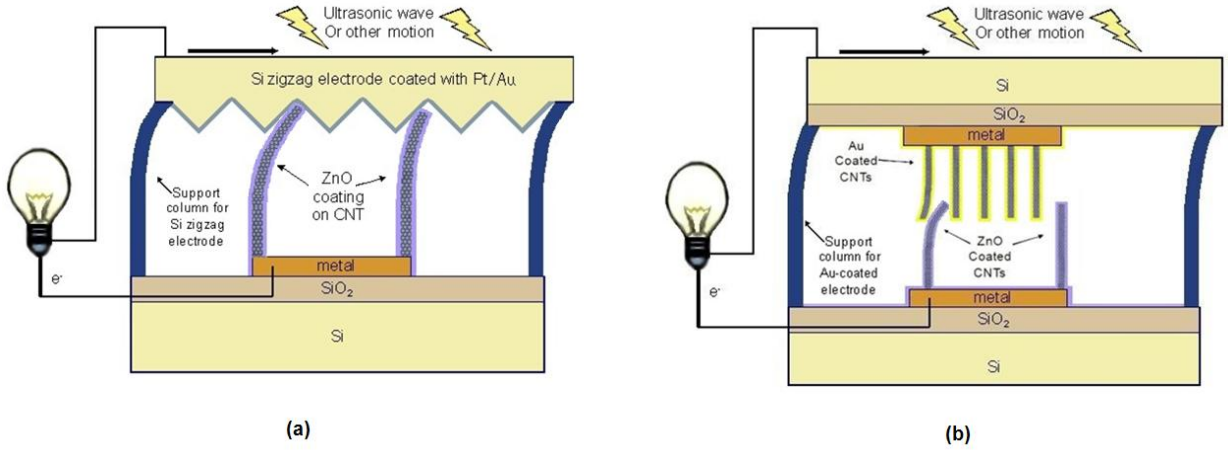


Figure 6. Schematics of Si wafer-based nanogenerators with conductive electrodes formed from a) an anisotropically etched Si wafer and b) a CNT carpet, adapted from [18]

The piezoelectric generator design based on a flexible substrate relies on CNTs grown onto a flexible woven carbon fiber fabric (Figure 7). ZnO and gold are then deposited on separate CNT-coated carbon fiber sheets, which may be combined in alternating layers. This would produce a flexible network of energy generating conductors that could potentially be incorporated into any number of technologies, such as electronically functionalized clothing or military gear and energy recuperative tires.

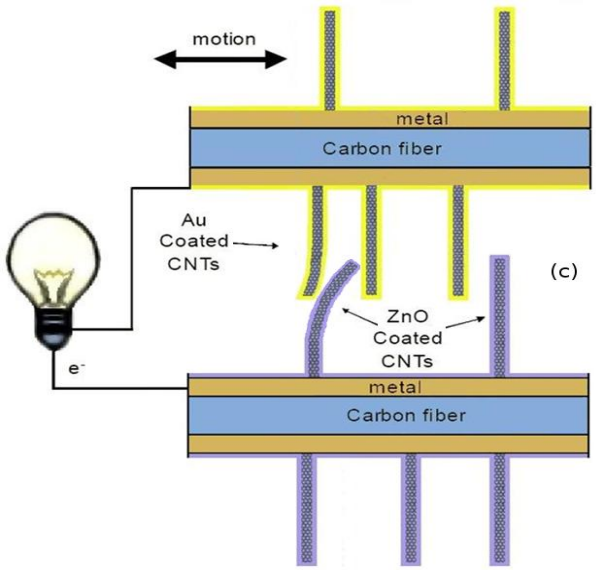


Figure 7. Schematics of carbon fiber weave-based nanogenerators CNTs coated in ZnO and gold to form piezoelectric and conductive electrodes, adapted from [18]

**CNT Growth and Photolithographic Patterning:**

Iron must first be deposited on the substrate for use as a catalyst in CNT growth. Samples were placed in a Denton Vacuum Thermal Evaporator bell chamber approximately 10 cm from the source position on a rotating platform. A length of 99.9999% purity iron wire, weighing approximately 0.01g, was affixed to a tungsten filament by wrapping tightly upon itself to approximate a point source. The chamber was pumped down to ~$4x10^{-6}$ Torr. Voltage was increased 50% max output, corresponding to a maximum filament current of ~30A and held for 3 seconds then immediately decreased to zero. This caused the iron wire to evaporate, depositing a 100nm layer on the samples.

The CNTs may then be grown on either substrate type in a FIRST NANO CVD furnace chamber using a standard recipe, according to the following process parameters:

- Ramp temperature up to 825˚C over 10 min
- Hold for 30 min with gas flow of 130 sccm of $C_2H_2$, 1,000 sccm of $CH_4$, and 500 sccm of $H_2$
- Purge CVD chamber and cool to below 200˚C in 1,000 sccm argon flow

Photolithographic patterning of the iron catalyst may be performed prior to CNT growth. The photolithographic procedure used was as follows:

- Clean wafer with TCE, methanol, acetone, DI water
- Spin coat photoresist (PR1818) for 5000 RPM for 25 sec
- Bake at 95˚C for 30 min
- Align mask and expose with 274.5 nm light for 6.5 sec
- Soak in chlorobenzene for 10 min
- Blow dry using $N_2$
- Bake at 95˚C for 10 min
- Develop (using 70:20 mL mixture of DI water:developer 351) for 60 sec
- After inspection, strip photoresist in solvent (acetone) for 30 min while sonicating (optional)

Patterning the catalyst deposited on the silicon wafers should create space for the coated CNTs to bend in order to create optimal charge generation and collection at the Schottky barrier. The increase in spacing between CNTs should also allow greater ZnO and gold penetration through the CNTs during deposition.

The quality of CNT growth on the patterned wafer substrates fabricated thus far has not been ideal. The small number of CNTs produced may be due to over-oxidation of the iron catalyst. Further attempts will require less time between processing steps—moving from iron catalyst deposition, to photoresist liftoff, then straight to CNT growth. Previous CNT growth utilizing carbon fiber as the substrate produced CNTs of standard length that were not well aligned [39]. Attempts to produce shorter CNTs during this project have resulted in very little CNT growth on the carbon fiber (Figure 8).

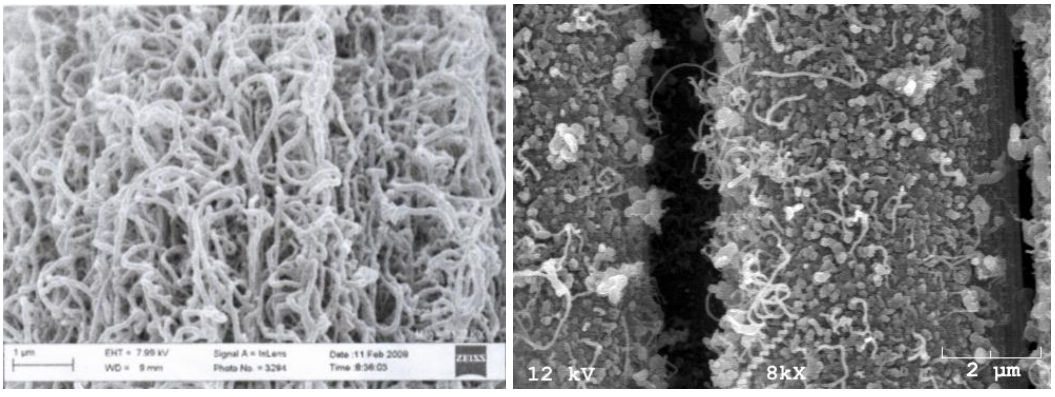


Figure 8. CNTs grown on carbon fiber substrates. Unaligned, standard length CNTs [39] (left) grew better than the shorter length CNTs (right).

Further attempts to modify the CNT growth parameters must be made in order to determine a growth recipe for use with carbon fiber as a substrate that can produce CNTs with adequate alignment.

**ZnO and Gold Film Deposition:**

In order to optimize the piezoelectric effect of the ZnO coating, the deposited film should be single crystal or polycrystalline with a specific preferred orientation. The complex, nonplanar geometry of the substrate makes this process difficult. Of the two methods already used—IAD [46] and RF sputtering [47]—the sputtered film has produced the most preferred orientation thus far. A two step sputtering deposition process has been identified which may improve its quality. This method relies on growth of a high quality seed layer of ZnO at a slow rate of deposition using 50W power or less, followed by fast epitaxial growth upon that layer at a higher power of 150W with gas flow of 6 mTorr using 50% $O_2$/50% Ar mix.

The patterned samples, referred to above, were used in a second deposition of ZnO by IAD, with process parameters altered to improve the depth of ZnO permeation into the CNT carpet:

| | **ZnO IAD 1:** | **ZnO IAD 2:** |
|---|---|---|
| **Thickness** | 100 nm | 150 nm |
| **Deposition substrate temperature** | 50˚C | 50˚C |
| **Deposition rate** | 0.2 nm/s | 0.1 nm/s |
| **$O_2$ flow rate** | 5 sccm | 5 sccm |
| | **Plasma parameters** | |
| **Bias voltage** | 110 V | 125 V |
| **Discharge current** | 45 A | 50A |
| **Ar gas 1 flow rate** | 2 sccm | 4 sccm |
| **Ar gas 2 flow rate** | 14 sccm | 16 sccm |

The strength of adhesion of the gold film upon the CNTs has not yet been determined. Gold often requires an additional buffer or “adhesion layer” in

order to remain firmly attached when deposited on many substrates [48-49]. The addition of a titanium adhesion layer before gold deposition may be necessary. The gold electrode as it comes into contact with a ZnO surface that has built up charge on it is like that of a diode. The Schottky barrier will allow charge to flow in one direction only—away from the ZnO film, generating current. The addition of this Ti layer is not likely to interfere with the Schottky behavior of the gold electrode.

Attempts to verify adhesion of the ZnO and gold films on the CNTs by a scratch test were inconclusive due to the lift off of the CNTs themselves. The durability of the deposited CNTs at the point of contact with the silicon wafer substrate may be a weak point as well. A tape adhesion test was used to determine the point of failure of the samples when placed in tension. They were tested by placing the coated ends of CNT samples onto a conductive adhesive SEM tab, then peeling them off. A section of the wafer with CNTs separated was also placed on the SEM stub, for comparison. Samples of sputtered Au, thermally evaporated Au, sputtered ZnO and IAD ZnO were imaged with the Hitachi S800 SEM to determine the point of failure from substrate to coating (see Figures 9-16).

**Electrical testing:**

Preliminary tests were performed using a Keithley 619 electrometer/multimeter with picoampere scale sensitivities to determine the charge generated from devices composed of electrodes built using either the rigid or the flexible substrate. For each substrate type, specimens produced through differing process parameters have been combined to determine optimum charge generation. For the rigid, wafer-based substrates, a combination of a ZnO-coated, patterned CNT array electrode and gold-coated, carpet-grown CNTs electrode were expected to produce the best results. The patterned conductive electrodes should isolate and efficiently deform the ZnO-

coated CNTs, while providing ample opportunity to dissipate the charge produced.

The electrical testing performed with a Keithley multimeter could not produce real-time data while the force was applied to the nanogenerator because measurement had to be recorded manually. New testing equipment has become available to take real-time electrical measurements of the nanogenerators, with the addition of energy in the form of ultrasonic waves. Electrodes combined in this configuration must first be altered by embedding the two electrodes into a watertight sealant, such as epoxy, with the attached testing leads exposed. The first samples created by this method were measured with a Keithley 4200 SCS, resulting in measurement of current and voltage with applied energy from sonication (Figure 7).

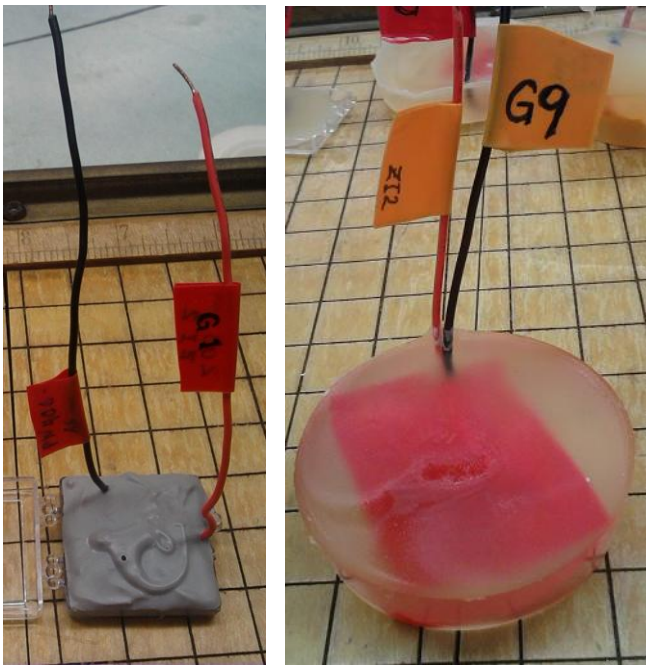


Figure 7. Nanogenerator electrodes were embedded in two types of epoxy to seal against water used during measurement in sonicator.

Additional epoxy sealed nanogenerator samples have been prepared and tested with a picoammeter, both in and out of a sonicator. This is necessary to determine whether they remained in electrical contact, have been adequately sealed, and to compare to previous testing of multiple combinations with the

Keithley multimeter. These samples were tested to determine current output before they were embedded (while in the configuration shown in Figure 3b), after they had been embedded in epoxy, and once they had been cured. For the samples within the sonicator, the sonication frequency was increased, and the resulting current output was measured. The additional nanogenerators were tested using a different Keithley 4200 SCS setup (Figure 8).

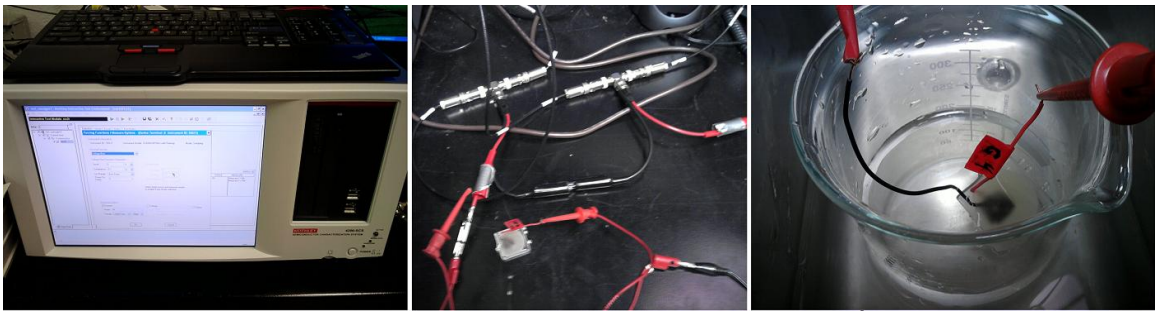

Figure 8. Keithley 4200SCS (left), cables used during testing (middle), sample G4 suspended in water within the sonicator (right)

## Results and Discussion

### Film Quality:

The quality of the sputtered gold film was superior to the film fabricated by thermal evaporation. The sputtered film was visibly thicker, even though 30nm layers should have been deposited on each sample (Figure 9).

Figure 9. Electrodes produced by coating CNTs with gold by sputtering and evaporation (left), sputtered Au coating (middle), and evaporated Au coating (right).

These films did not fully permeate to the CNT bases due to shadowing at the CNT tips.

Both the gold and ZnO coatings from initial deposition runs were found to have penetrated into the tops of the CNT arrays 2-10 μm of the approximately 50-60 μm length CNTs (Figure 10).

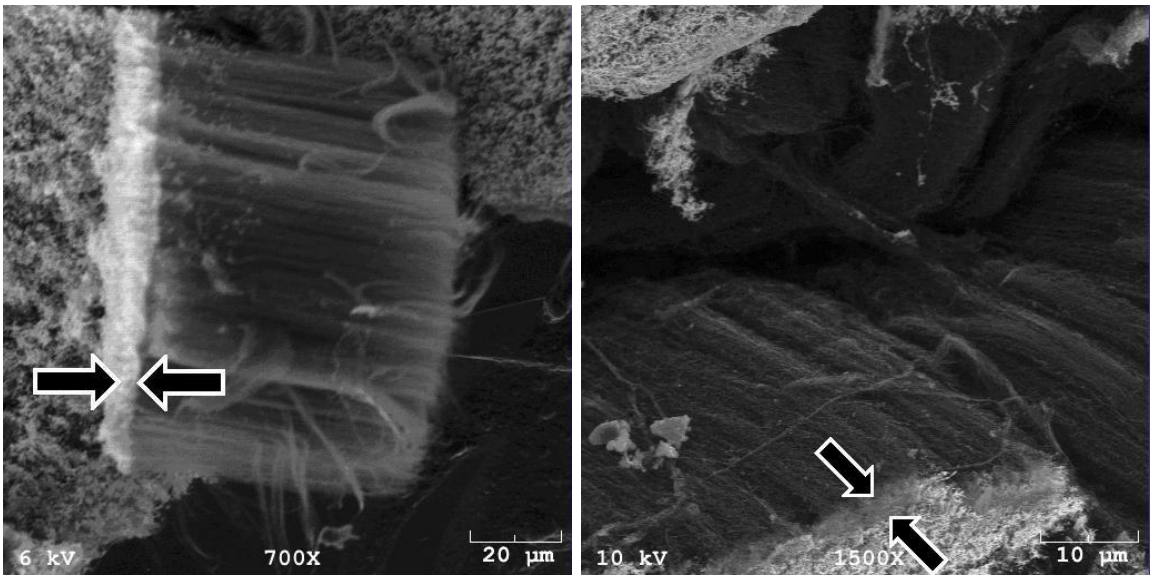


Figure 10. CNTs grown on a silicon wafer were deposited with ZnO film (left, indicated by arrows) using IAD, and gold film (right, indicated by arrows) using e-beam evaporation.

It was determined that evaporation of gold and IAD of ZnO were not adequate means of deposition onto such high profile (large aspect ratio) features as CNTs. Evaporation is a line of sight process, so the tips of the CNTs likely "shaded" the remainder of the deposition—effectively building up deposited material only at the surface, rather than penetrating to the length of the CNTs.

Theoretically, IAD, which is essentially e-beam evaporation with the addition of plasma that sputters (not a line of sight process) the sublimated material at the substrate surface, may be able to overcome this shading effect by use of a higher power plasma and longer deposition time to produce a more uniform, conformal film. The first ion-assisted deposition run did not result in conformal coating of the CNTs. Results from the second deposition showed no noticeable change in ZnO permeation. The energy from the plasma did not effectively

increase the coverage of the ZnO deposition over the length of the carbon nanotubes (Figure 11).

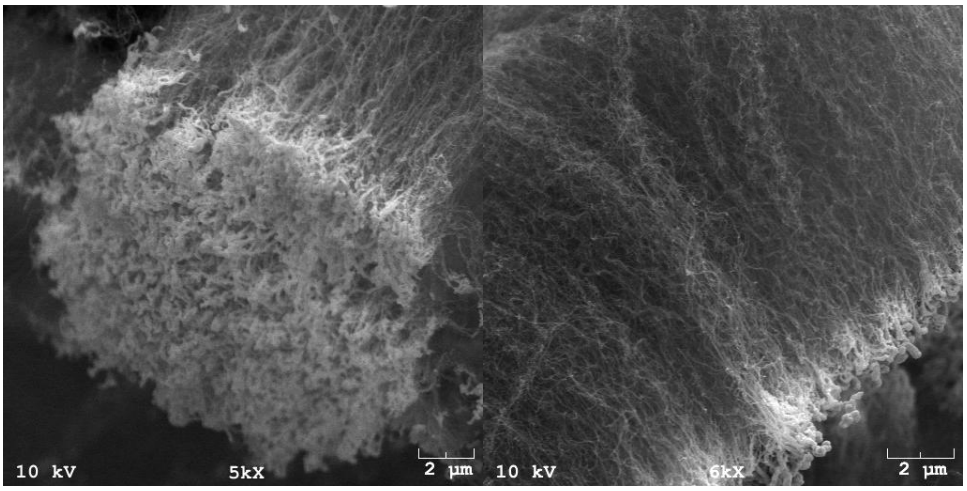


Figure 11. CNTs coated in ZnO by IAD; first deposition run (left), and second run (right).

The ZnO coatings produced by sputtering provided greater uniformity and crystal quality than those produced by IAD (Figure 11).

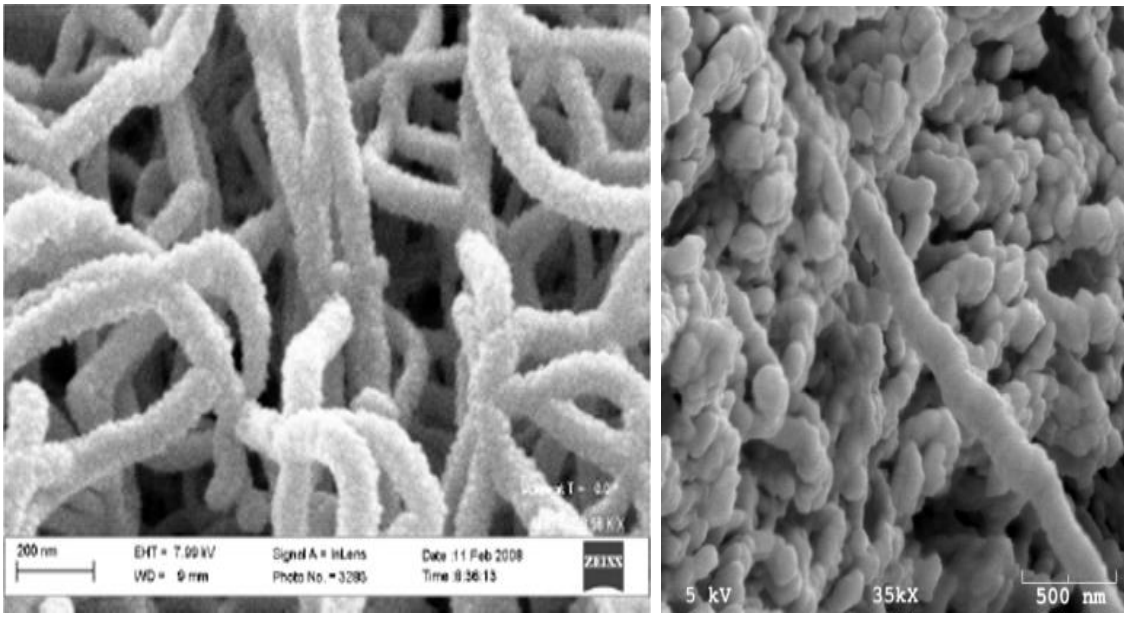


Figure 12. Quality of ZnO coatings on CNTs deposited by sputtering [39] (left), and IAD (right).

Because the growth of the patterned CNTs was so poor, it cannot yet be determined whether the openings in the CNT carpet (space between features)

would have provided enough access to the CNT base region in order to fully coat them with ZnO or gold.

**Adhesion:**

Figures 13-17 show the CNTs separated from the wafer by a tape adhesion test and Figures 18-19 show the CNTs that remained on the wafer. Nanotubes of approximately 15 μm in length are shown in Figure 19, a portion of which have been pressed at an angle from the rest of the carpet either during or after separation from the wafer.

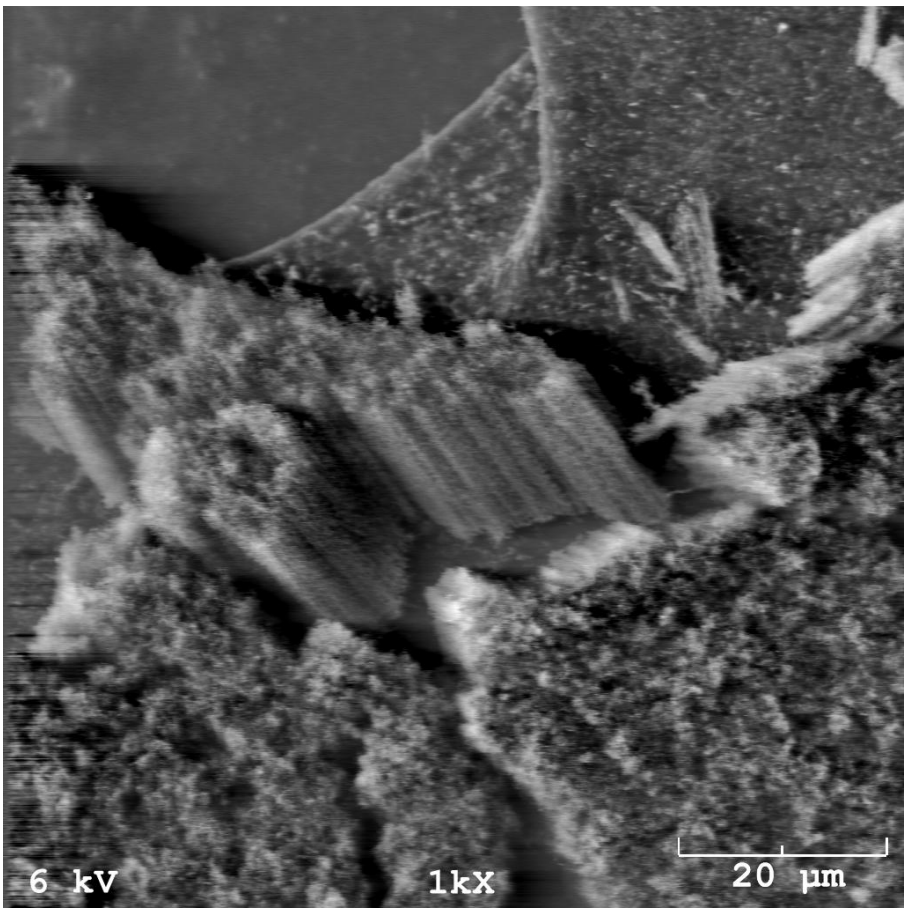


Figure 13. Au coated CNTs separated from silicon wafer

Regions surrounding a hole in the adhesive SEM tab were less likely to provide contact positions for the CNT carpet. Figure 14 is a low magnification view of such a region, with further images of increasing magnification of the area

where a substantial amount of ZnO-coated CNT tips remained (boxed region). Images are shown in greater magnification in Figures 15-17.

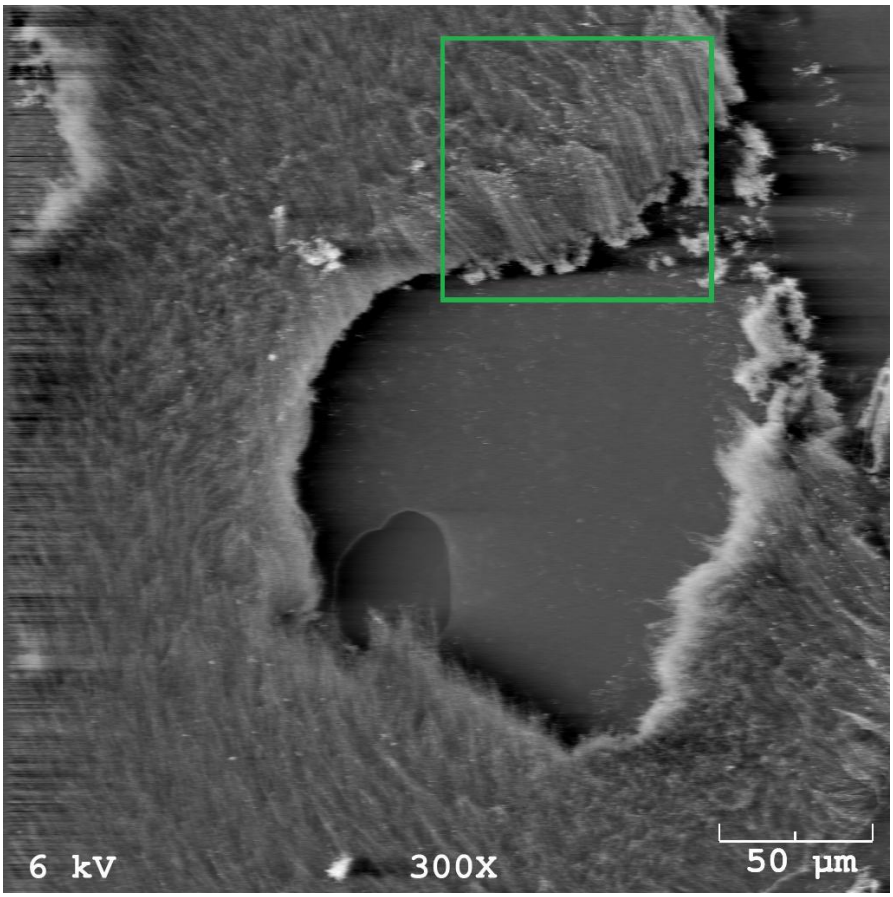


Figure 14. ZnO deposited CNTs separated from silicon wafer

ZnO-coated CNTs of approximately 20 microns (in the boxed region) are shown in Figure 15. The mat appears to be pressed at an angle as well. ZnO-coated tips alone are present along the bottom, clustered in bundles on the right. There are scattered particulates present at the bases of the CNTs which may be the remains of the ZnO coatings at the CNT tips. This suggests that the CNTs themselves are not broken, but the CNT/ZnO coating bond or the point where initial CNT growth occurred on the substrate is the weakest point.

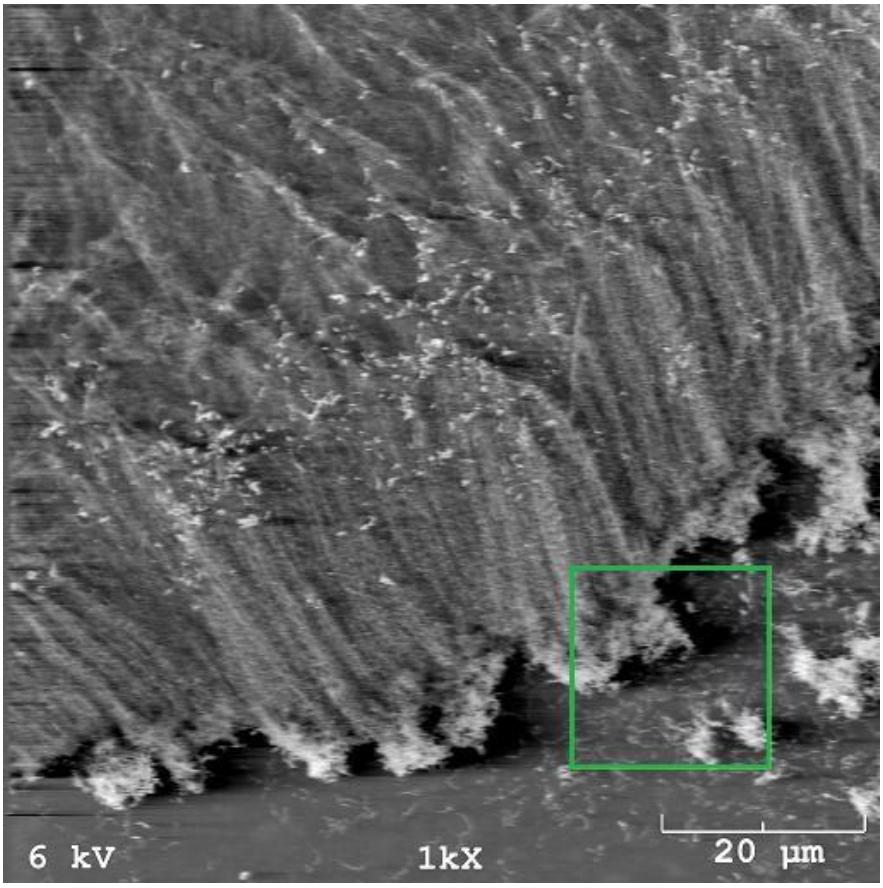

Figure 15. ZnO-coated CNTs separated from silicon wafer. This image is a subset of Fig. 14

Figures 16 and 17 present a more detailed view of the ZnO-coated tips of the CNTs, both detached and attached to the CNT carpet. The lighter coloration due to charging of the remaining tips suggests that the point of failure is somewhere within the region of the ZnO-CNT interface. Short (~2 µm) lengths of ZnO-coated CNT remain embedded in the SEM tab adhesive.

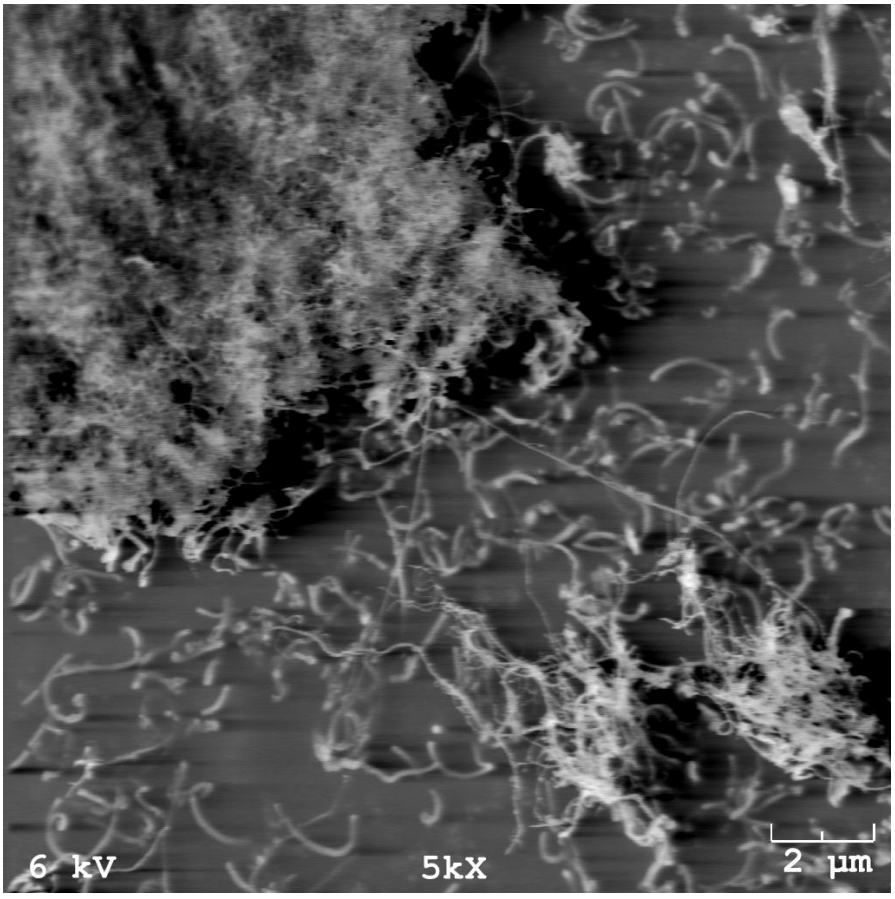


Figure 16. ZnO-coated CNTs separated from silicon wafer (subset of Figure 15)

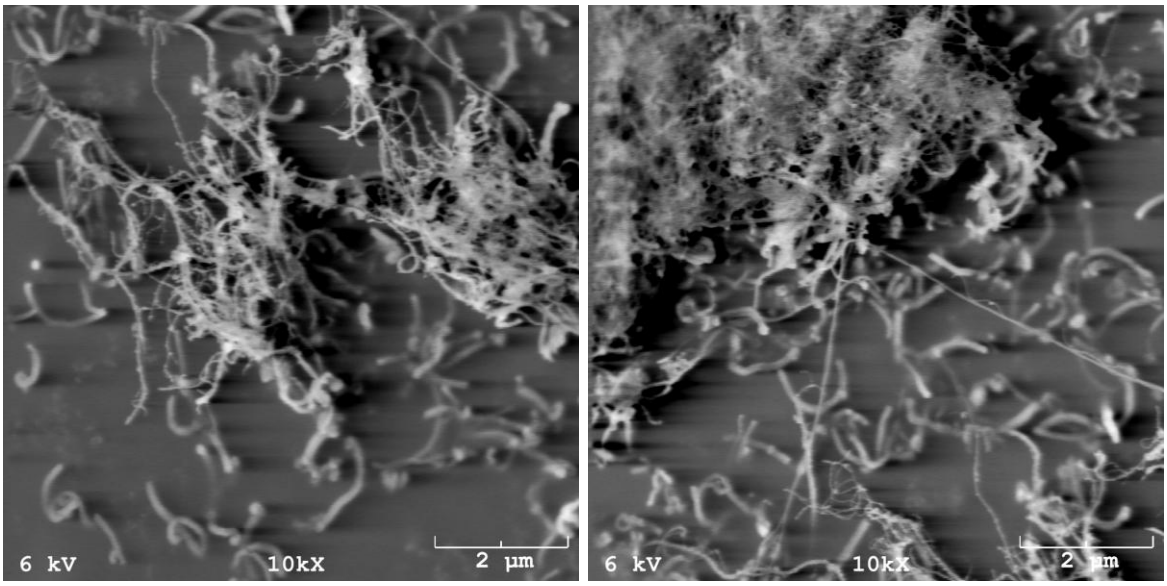


Figure 17. Higher magnification portions of above image (Fig.16)

A section of the ZnO-coated CNT carpet that remained on the wafer (did not adhere to the SEM tab) is shown in Figure 18. The CNTs that did not adhere were of varying lengths, suggesting a strong CNT/substrate bond.

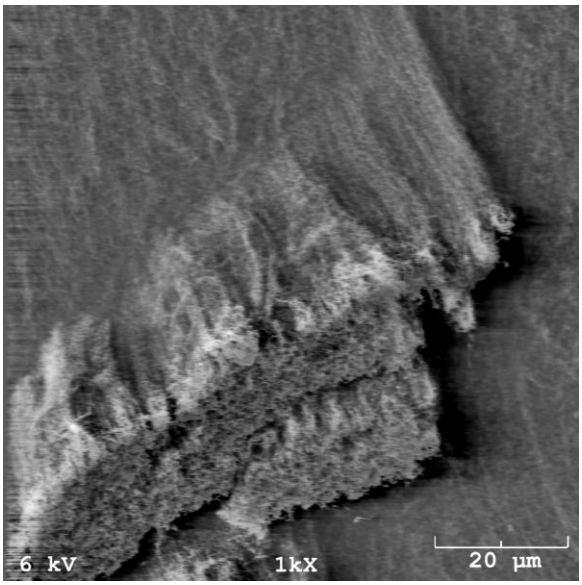


Figure 18. ZnO-coated CNTs remaining attached on the silicon wafer

The remaining sections of gold-coated CNT carpets on Si wafers are shown in Figure 19. The full, 60 µm length CNTs have been shredded at the mat's edge (left), while broad regions of the CNT mat appear to be torn from the wafer at varying lengths (right) close to the edge of the wafer .

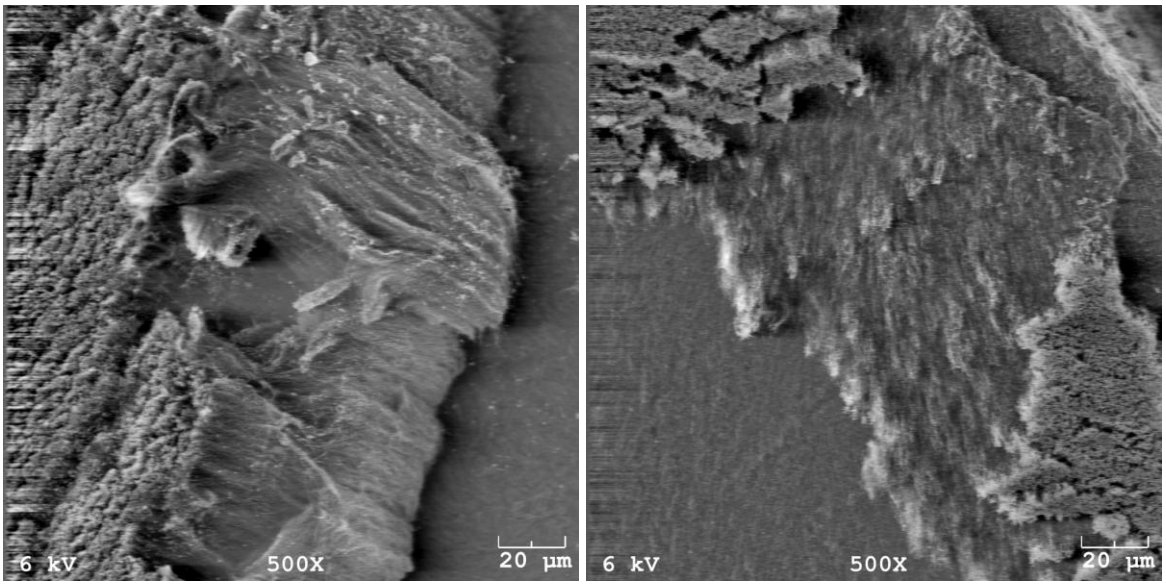


Figure 19. Full length (left) and torn (right) Au coated CNTs remaining attached on silicon wafer

Adhesion may be improved if the films deposited on the CNTs were to coat them uniformly (down to the substrate).

**Electrical Testing:**

Preliminary tests performed using a Keithley 619 electrometer/multimeter indicate that the carbon fiber substrate-based electrodes produce the highest power output (significant values are bold in Table 1).

Table 1. Initial electrical measurements of various nanogenerator configurations

| Electrodes | | Current [nA/cm$^2$] | Current [nA/cm$^2$] | Voltage [μV] | Power [pW] |
|---|---|---|---|---|---|
| Top & Bottom coating | Patterning & Substrate | Contact only* | Light pressure | Light pressure | Light pressure |
| **evaporated Au + IAD ZnO** | **carpet / carpet on Si wafer** | **32** | **49** | **46** | **2.50** |
| sputtered Au + IAD ZnO | carpet / carpet on Si wafer | 100 | 130 | 16 | 2.08 |
| sputtered Au + IAD ZnO | line & ring arrays on Si | 92 | 112 | 25 | 2.80 |
| sputtered Au + IAD ZnO | line & ring arrays on Si | 1.5 | 1.8 | 33 | 0.06 |
| sputtered Au + IAD ZnO | line / line arrays on Si wafer | 4 | 5 | 7 | 0.04 |
| sputtered Au + IAD ZnO | ring array & carpet on Si | 60 | 145 | 20 | 2.90 |
| **sputtered Au + IAD ZnO** | **carpet/carpet on carbon fiber** | **120** | **130** | **45** | **5.85** |
| **sputtered Au + IAD ZnO** | **carpet on carbon fiber & Si wafer** | **160** | **280** | **6** | **1.68** |
| **Al + Cu foil** | | 55 | 173 | 0.167 | 0.29 |

* No pressure applied apart from influence of gravity

Electrical measurements of the first prototype ZnO-coated CNT based piezoelectric nanogenerators produced currents up to 0.28 μA/cm$^2$. The testing of copper and aluminum electrodes by these same methods produces measurements of similar magnitudes, which suggests that these values may not be reliable indicators of piezoelectric generation or charge. These values could

potentially be increased with better penetration of both gold and ZnO coatings during deposition on the CNTs. Increases in the film quality characteristics, such as gold adhesion and ZnO crystal orientation, as well as improvements through patterning and conductive electrode design may also increase current generation.

Initial tests utilizing software that provides real-time measurements of the electrical output of the nanogenerators under applied stress have been performed using a Keithley 4200 SCS. It has been determined that the generated current is the result of application of stress to the nanogenerator—indicating the presence of a piezoelectric effect. Current and voltage measurements from the first tests conducted in a sonicator are displayed in Figures 20 and 21. These measurements were taken during testing of sample G1—a combination of electrodes produced by photolithographic patterning of CNTs, then coating in gold by sputtering with carpet grown CNTs coating by IAD of ZnO. The current produced shows positive and negative values as the testing leads are switched.

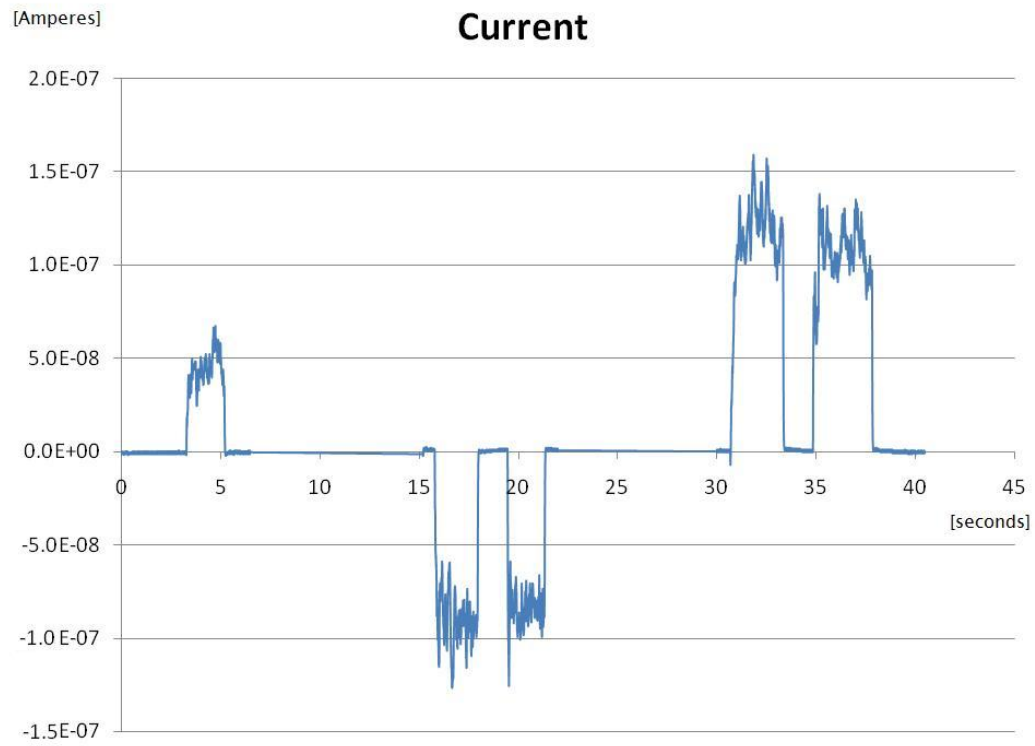


Figure 20. Current generated from gold coated CNT/ZnO-coated CNT nanogenerator

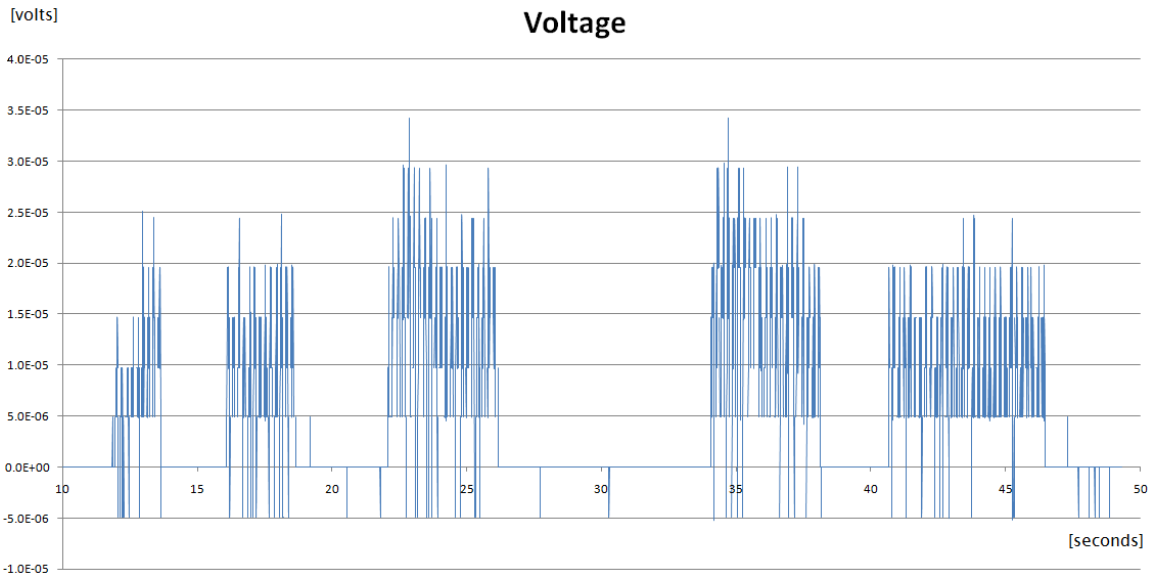


Figure 21. Voltage versus time measured during testing of nanogenerator corresponding to ultrasonic pulses.

Additional epoxy sealed nanogenerator samples have been prepared and tested with a picoammeter in and out of a sonicator to determine whether they remained in contact, have been adequately sealed, and produce comparable current to previous testing of multiple combinations with the Keithley multimeter. Output currents are displayed in Table 2, with electrode information provided in the key following the table.

Table 2. Initial electrical measurements of various nanogenerator configurations

| | | | Before embedding | Embedded, outside sonicator | Embedded, in sonicator |
|---|---|---|---|---|---|
| Sample # | Electrode 1 | Electrode 2 | I [nA] | I [nA] | I [nA] |
| **G1** | **PW406_AS** | **SW205_ZI2** | **1.20 – 1.45** | | **1.13 - 1.20** |
| G4 | SW203.2_ZI2 | | 1.55 | 1.28 | 1.66 |
| G5 | SW501_ZS1i | | 1.33 | | 1.15 - 1.08 |
| G7 | SW105_AS | | 89 - 117 | 0.99 - 1.13 | 1.00 - 1.13 |
| **G8** | **SW103_AE** | **SW502_ZS1i** | **155 - 188** | **19.9 - 190** | **190 - 1200** |
| G9 | SW503_ZS2i | SW504_ZS2i | 168 - 199 | 50 - 1.13 | 1.13 - 88 |
| G10 | PW405_AS | TW303_ZI2 | 1.40 | 1.33 | 1.13 - 1.03 |
| G11 | PW311_AE | PW317_AE | 1.35 | 0.66 | 0.50 - 0.66 |

**Table 2 Key:**
PW/TW – patterned CNTs on wafer
SW - carpet CNTs on wafer
AS - sputtered Au coating
AE - evaporated Au coating
ZS(1i/2i) - sputtered ZnO coating (inches from center during deposition)
Z(I2) - IAD coated, 2nd run

The base level current recorded by the picoammeter was affected by testing conditions. When the system was sitting untouched the current measured averaged 0.009 nA. When the alligator clips alone were being handled (before attachment to the nanogenerator) the current rose to approximately 0.4 nA.

The increase in sonicator frequency did not correlate directly to changes in current produced but the values did vary throughout testing for some samples. The highest current produced was 1.2 μA from sample G8- a combination of carpet CNTs on silicon, coated in IAD ZnO and evaporated gold. The increased values from the new electrodes when testing with the picoammeter suggest that they may generate as much or more current when real-time measurements are taken within the sonicator.

Measured current produced from sample G4, tested using the Keithley system in Figure 8, is displayed in Figure 22. The same reversal of polarity is evident, as with the measurements shown in Figure 20, as a result of the sample terminals being switched while testing during sonication.

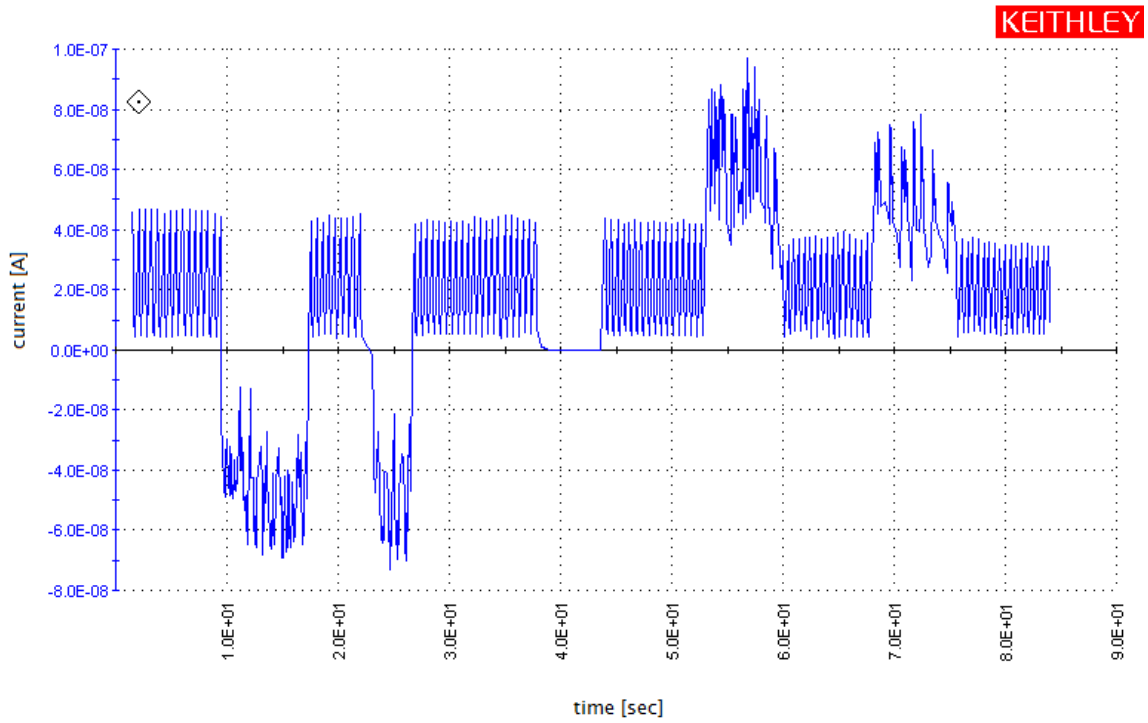


Figure 22. Current generated during sonication of sample G4 showing polarity reversal

## Conclusion

None of the deposition techniques employed to coat ZnO or gold on the CNT-based electrodes fabricated thus far have been able to permeate through the CNT carpet to the Si wafer base. However, these electrodes have been shown to produce verifiable current upon application of stress or deformation resulting from ultrasonic waves. Adequate electrical measurements have not been performed on a large enough sample selection to draw broad conclusions about the quality of the films used to fabricate the electrodes, but it is clear that the configurations currently used are capable of generating current and that those current levels may be improved upon. The point of failure of the electrode resulting from adhesion testing is mostly localized at the CNT/catalyst/substrate interface. More conformal, higher quality ZnO and gold coatings will provide better current generation as well as greater mechanical stability.

## Future Work

Production of additional electrodes using all processing variable combinations should be continued to ascertain reproducibility of results, this includes: additional gold coated electrodes (deposition by sputtering and evaporation), and zinc oxide coated electrodes (deposition by RF sputtering and IAD, as well as sol-gel, thermal evaporation and CVD) with samples of each coated CNT type on Si wafer, patterned Si wafer, and carbon fiber substrates. Improvement of current output may be accomplished by better isolation of the CNTs through photolithographic patterning, better aligned growth, and/or a conductive electrode in the form of a zigzag grating. These electrodes may then be combined, embedded in epoxy, and electrically tested in a sonicator. Additional characterization, in the form of SEM of samples, post-testing, may be necessary, as well as further characterization of the films by TEM, and XRD to ascertain the chemical composition and structure of the coatings.

## References


[1] Lefeuvre, E., A. Badel, C. Richard, L. Petit, and D. Guyomar, "A comparison between several vibration-powered piezoelectric generators for standalone systems," *Sensors and Actuators A: Physical,* vol. 126, pp. 405-416, 2006.

[2] Beeby, S. P., M. J. Tudor, and N. M. White, "Energy harvesting vibration sources for microsystems applications," *Measurement Science and Technology,* p. R175, 2006.

[3] Sodano, H. A., D. J. Inman, and G. Park, "Comparison of Piezoelectric Energy Harvesting Devices for Recharging Batteries," *Journal of Intelligent Material Systems and Structures,* vol. 16, pp. 799-807, October 1, 2005 2005.

[4] Roundy, S., E. S. Leland, J. Baker, E. Carleton, E. Reilly, E. Lai, B. Otis, J. M. Rabaey, P. K. Wright, and V. Sundararajan, "Improving power output for vibration-based energy scavengers," *Pervasive Computing, IEEE,* vol. 4, pp. 28-36, 2005.

[5] Renaud, M., T. Sterken, P. Fiorini, R. Puers, K. Baert, and C. van Hoof, "Scavenging energy from human body: design of a piezoelectric transducer," in *Solid-State Sensors, Actuators and Microsystems, 2005. Digest of Technical Papers. Transducers '05. The 13th International Conference on*, 2005, pp. 784-787 Vol. 1.

[6] Jeon, Y. B. , R. Sood, J. H. Jeong, and S. G. Kim, "MEMS power generator with transverse mode thin film PZT," *Sensors and Actuators A: Physical,* vol. 122, pp. 16-22, 2005.

[7] Ericka, M., D. Vasic, F. Costa, G. Poulin, S. Tliba "Energy harvesting from vibration using a piezoelectric membrane," *Journal de Physique IV,* vol. 128, pp. *187-193*, 2005.

[8] Cornwell, P. J., J. Goethal, J. Kowko, and M. Damianakis, "Enhancing Power Harvesting using a Tuned Auxiliary Structure," *Journal of Intelligent Material Systems and Structures,* vol. 16, pp. 825-834, October 1, 2005 2005.

[9] Roundy, S. and P. K. Wright, "A piezoelectric vibration based generator for wireless electronics," *Smart Materials and Structures,* p. 1131, 2004.

[10] Richards, C. D., M. J. Anderson, D. F. Bahr, and R. F. Richards, "Efficiency of energy conversion for devices containing a piezoelectric component," *Journal of Micromechanics and Microengineering,* p. 717, 2004.

[11] Poulin, G., E. Sarraute, and F. Costa, "Generation of electrical energy for portable devices: Comparative study of an electromagnetic and a piezoelectric system," *Sensors and Actuators A: Physical,* vol. 116, pp. 461-471, 2004.

[12] Bayrashev, A., W. P. Robbins, and B. Ziaie, "Low frequency wireless powering of microsystems using piezoelectric-magnetostrictive laminate composites," *Sensors and Actuators A: Physical,* vol. 114, pp. 244-249, 2004.

[13] Gonzalez, J.L., A. Rubio, F. Moll, "A prospect of the piezoelectric effect to supply power to wearable electronic devices" in *Proc. 4th Int. Conf. on Materials Engineering for Resources Akita, Japan*, pp. 202-07, 2001.

[14] Allen, J. J., and A. J. Smits, "Energy harvesting eel," *Journal of Fluids and Structures,* vol. 15, pp. 629-640, 2001.

[15] Goldfarb, M., and L. D. Jones, "On the Efficiency of Electric Power Generation With Piezoelectric Ceramic," *Journal of Dynamic Systems, Measurement, and Control,* vol. 121, pp. 566-571, 1999.

[16] Kawai, Y., "The Piezoelectricity of Poly (vinylidene Fluoride)," *Japanese Journal of Applied Physics,* vol. 8, pp. 975-976 1969.

[17] Umeda, M., K. Nakamura, S. Ueha, "Analysis of the Transformation of Mechanical Impact Energy to Electric Energy Using Piezoelectric Vibrator," *Japanese Journal of Applied Physics*. vol 35, pp. 3267–3273, 1996.

[18] Stollberg, D.W., "Nanogenerators from Piezoelectric-coated Carbon Nanotubes," white paper, GTRI, 2008.

[19] Wang, X., J. Song, J. Liu, Z. L. Wang, "Direct-Current Nanogenerator Driven by Ultrasonic Waves," *Science,* vol. 316 no. 5821, pp. 102, April 2007.

[19] Yang, R., Y. Qin, C. Li, L. Dai, Z. L. Wang, "Characteristics of output voltage and current of integrated nanogenerators," *Applied Physics Letters,* vol. 94, pp. 022905-3, 2009.

[20] Gao, Y., and Z. L. Wang, "Equilibrium Potential of Free Charge Carriers in a Bent Piezoelectric Semiconductive Nanowire," *Nano Letters,* vol. 9, pp. 1103-1110, 2009.

[21] Zhou, J., P. Fei, Y. Gu, W. Mai, Y. Gao, R. Yang, G. Bao, Z. L. Wang, "Piezoelectric-Potential-Controlled Polarity-Reversible Schottky Diodes and Switches of ZnO Wires," *Nano Letters,* vol. 8, pp. 3973-3977, 2008.

[22] Z. L. Wang, X. Wang, J. Song, J. Liu, Y. Gao, "Piezoelectric Nanogenerators for Self-Powered Nanodevices," *Pervasive Computing, IEEE,* vol. 7, pp. 49-55, 2008.

[23] Z. L. Wang, "Towards Self-Powered Nanosystems: From Nanogenerators to Nanopiezotronics," *Advanced Functional Materials,* vol. 18, pp. 3553-3567, 2008.

[24] J. Song, X. Wang, J. Liu, H. Liu, Y. Li, and Z. L. Wang, "Piezoelectric Potential Output from ZnO Nanowire Functionalized with p-Type Oligomer," *Nano Letters,* vol. 8, pp. 203-207, 2008.

[25] Y. Qin, R. Yang, and Z. L. Wang, "Growth of Horizontal ZnO Nanowire Arrays on Any Substrate," *The Journal of Physical Chemistry C,* vol. 112, pp. 18734-18736, 2008.

[26] Y. Qin, X. Wang, and Z. L. Wang, "Microfibre-nanowire hybrid structure for energy scavenging," *Nature,* vol. 451, pp. 809-813, 2008.

[27] J. Liu, P. Fei, J. Zhou, R. Tummala, and Z. L. Wang, "Toward high output-power nanogenerator," *Applied Physics Letters,* vol. 92, p. 173105, 2008.

[28] J. Liu, P. Fei, J. Song, X. Wang, C. Lao, R. Tummala, and Z. L. Wang, "Carrier Density and Schottky Barrier on the Performance of DC Nanogenerator," *Nano Letters,* vol. 8, pp. 328-332, 2008.

[29] Y.-F. Lin, J. Song, Y. Ding, S.-Y. Lu, and Z. L. Wang, "Piezoelectric nanogenerator using CdS nanowires," *Applied Physics Letters,* vol. 92, p. 022105, 2008.

[30] Z. L. Wang, "The new field of nanopiezotronics," *Materials Today,* vol. 10, pp. 20-28, 2007.

[31] Y. Gao and Z. L. Wang, "Electrostatic Potential in a Bent Piezoelectric Nanowire. The Fundamental Theory of Nanogenerator and Nanopiezotronics," *Nano Letters,* vol. 7, pp. 2499-2505, 2007.

[32] J. S. P. X. Gao, J. Liu, Z. L. Wang,, "Nanowire Piezoelectric Nanogenerators on Plastic Substrates as Flexible Power Sources for Nanodevices," *Advanced Materials,* vol. 19, pp. 67-72, 2007.

[33] J. Song, J. Zhou, and Z. L. Wang, "Piezoelectric and Semiconducting Coupled Power Generating Process of a Single ZnO Belt/Wire. A Technology for Harvesting Electricity from the Environment," *Nano Letters,* vol. 6, pp. 1656-1662, 2006.

[34] Z. L. Wang and J. Song. “Piezoelectric Nanogenerators Based on Zinc Oxide Nanowire Arrays,” *Science,* vol. 312, no. 5771, p.242, April 2006.

[35] Iijima, S. “Helical Microtubules of Graphitic Carbon,” *Nature*, 354.6348 p. 56, 1991.

[36] S. Turano and J. Ready, "Chemical vapor deposition synthesis of self-aligned carbon nanotube arrays," *Journal of Electronic Materials,* vol. 35, pp. 192-194, 2006.

[37] J. F. Nye, *Physical Properties of Crystals,* Oxford: Oxford University Press, 1957.

[38] G. Sanborn. “Manufacture and Characterization of a Layered Carbon Fiber Material Covered with Carbon Nanotubes.” GTRI/SURF program, 2008

[39] Triboulet, R. and J. Perrière, "Epitaxial growth of ZnO films," *Progress in Crystal Growth and Characterization of Materials,* 2003. vol. 47, no. 2-3, pp. 65-138.

[40] Cheng, H.-C., C.-F. Chen, C.-Y. Tsayc, J.-P. Leua, "High oriented ZnO films by sol-gel and chemical bath deposition combination method," *Journal of Alloys and Compounds,* Vol.475, no. 1-2, pp. L46-L49, 2009.

[41] Lee, J., A.J. Eastealb, U. Palc, D. Bhattacharyyaa, "Evolution of ZnO nanostructures in sol-gel synthesis," *Current Applied Physics*, vol. 9, no. 4, pp. 792-796, 2009.

[42] Lin, L.-Y. and D.-E. Kim, "Effect of annealing temperature on the tribological behavior of ZnO films prepared by sol-gel method," *Thin Solid Films,* vol. 517, no. 5, p. 1690-1700, 2009.

[43] Chrissanthopoulos, A., S. Baskoutasa, N. Bouropoulosa, V. Dracopoulosb, D. Tasisa, S.N. Yannopoulosb "Novel ZnO nanostructures grown on carbon nanotubes by thermal evaporation," *Thin Solid Films*, vol. 515, no. 24, pp. 8524-8528, 2007.

[44] Kim, H. and W. Sigmund, "Zinc oxide nanowires on carbon nanotubes," *Applied Physics Letters*, vol. 81, no. 11: pp. 2085-2087, 2002.

[45] Frühauf, J. and S. Krönert, "Wet etching of silicon gratings with triangular profiles," *Microsystem Technologies,* vol. 11(12): pp. 1287-1291, 2005.

[46] Miyamoto, K., M. Yoshida, H. Toyotama, S. Onari, T. Arai. "ZnO Thin Films Prepared by Ion-Assisted Deposition Methods," *Japanese Journal of Applied Physics*, vol. 30, pp. 1830-1835, 1991.

[47] Hsu, Y.-H., J. Lin, and W. Tang, "RF sputtered piezoelectric zinc oxide thin film for transducer applications," *Journal of Materials Science: Materials in Electronics*, 19, no.7, pp. 653-661, 2008.

[48] Kishioka, S, J. Nishino, H. Sakaguchi, "Fabrication of Stable, Highly Flat Gold Film Electrodes with an Effective Thickness on the Order of 10 nm," *Analytical Chemistry,* vol. 79, no. 17, 6851-6856, 2007.

[49] Li, X., F. Huang, M. Curry, S.C. Street, M.L. Weaver, "Improved adhesion of Au thin films to SiOx/Si substrates by dendrimer mediation," *Thin Solid Films*, vol. 473, no.1, pp. 164-168, 2005.